ECS Transactions, 78 (1) 1367-1374 (2017)
10.1149/07801.1367ecst ©The Electrochemical Society

Study of $Sr_2MgMo_{0.9}Ni_{0.1}O_{6-\delta}$ as SOFC Anode

P. K. Dager[a], L.V. Mogni[a, b], G. Zampieri[a, b], A. Caneiro[a, b]

[a]Centro Atómico Bariloche (CAB) – Comisión Nacional de Energía Atómica (CNEA)
Av. Bustillo 9500 S.C. de Bariloche, CP 8400, Argentina
[b]Consejo Nacional de Investigaciones Científicas y Técnicas (CONICET)
Av. Rivadavia 1917 (C1033AAJ), Buenos Aires - Argentina

$Sr_2MgMo_{0.9}Ni_{0.1}O_{6-\delta}$ (SMMNi) double perovskite was synthesized by the combustion-solution method followed by annealing in air at 1100ºC for 12 hours. $Sr_2MgMoO_{6-\delta}$ (SMMO) compound was also tested for comparison. X-Ray Diffraction (XRD) patterns indicate that SMMO and SMMNi powders display triclinic symmetry. Thermogravimetric studies show that Mo-substitution by Ni in SMMO decreases the oxygen content in air condition. Meanwhile, after calcination in diluted-H_2 both compounds show oxygen non-stoichiometric change $\Delta\delta \approx 0.06$. EIS measurements on symmetrical SMMO/GDC/SMMO and SMMNi/GDC/SMMNi cells were performed in order to study the influence of time and environment conditions (H_2-content) on the anode polarization resistance (R_{pa}).

Introduction

Solid Oxide Fuel Cells (SOFCs) (1-3) are promising devices for efficient generation of electricity with an attractive flexibility in the selection of working fuel (H_2 and hydrocarbons) (4). The traditional Ni-based anodes used in SOFCs exhibit high efficiency when H_2 is used as fuel, but poor stability in redox cycles, and carbon deposition and sulfur poisoning when hydrocarbons are utilized (5). In the search of alternative anode materials to overcome these disadvantages, a ceramic mixed ionic-electronic conductor (MIEC) has been studied. The $Sr_2MgMoO_{6-\delta}$ (SMMO) double perovskite is a MIEC with high power densities when methane is used as fuel (6-8). This material is stable under reducing atmosphere at temperatures higher than 1000ºC and it shows good tolerance to sulfur poisoning. However, the electrical conductivity values reported for this material are lower than that of Ni-YSZ anodes. Therefore, the effects of the Mo-substitution by different cations in SMMO have been investigated with the purpose of improving the anode performance.

The W-doping in the Mo-site has little effects on crystal and redox chemistry of $Sr_2MgMoO_{6-\delta}$, but considerably depresses the electrical conductivity (9). In the same way, when Mo is replaced by Nb, the presence of excessive amounts of Nb^{5+} is also a drawback for the electrical conductivity. The above mentioned fact was attributed to a high oxygen deficiency and/or the fact that in $Sr_2MgMo_{1-x}Nb_xO_{6-\delta}$ only Nb (and not Mo) shows mixed valence. Besides, small amount of Nb would be useful when considering the materials as SOFC anode candidates (9), i.e. electrochemical studies, made on $Sr_2MgMo_{0.8}Nb_{0.2}O_{6-\delta}$ (10) in methane atmosphere, revealed that this oxide is active for

CO, CO_2 or C adsorption. Moreover, partial substitutions of Mo by V (11) in $Sr_2MgMo_{0.95}V_{0.05}O_{6-\delta}$ improved the catalytic activity and a stronger H_2S-tolerance in respect to $Sr_2MgMoO_{6-\delta}$ is obtained. Furthermore, it was observed that the V-doped compounds are more stable in methane than non-doped-samples.

In the present work, Mo was partially substituted by Ni in SMMO, in order to analyze its effect on crystal structure, and chemical and electrochemical properties of $Sr_2MgMo_{0.9}Ni_{0.1}O_{6-\delta}$ (SMMNi). These studies allow evaluating the potential use of SMMNi as anode material in SOFCs.

Experimental

Synthesis

$Sr_2MgMo_{0.9}Ni_{0.1}O_{6-\delta}$(SMMNi) and $Sr_2MgMoO_{6-\delta}$ (SMMO) were synthesized by the combustion-solution method (12-14). Stoichiometric amounts of $SrCO_3$ and Mg were dissolved in a diluted HNO_3 solution. MoO_3 was dissolved in a NH_4OH solution and a $Ni(NO_3)_26H_2O$-solution was dissolved in a diluted HNO_3 solution. Once the cations are in solution, the combustion procedure is similar to that reported for non-doped material (SMMO) (15). The ash-precursor was thermally treated under the optimized conditions of 1000ºC-12 h for SMMO and 1100ºC-12 h for SMMNi.

Characterization

X-Ray diffraction (XRD) measurements were collected at room temperature (RT) by using a Panalytical Empyrean diffractometer equipment with Cu-Kα radiation (λ = 0.1542 nm) and 3D PIXcel detector within $10º \leq 2\theta \leq 110º$ range. Rietveld refinements of the XRD patterns were performed by using FULLPROF tools (16).

Thermogravimetric analyses (TGA) were carried out in order to determine the oxygen content in oxidizing and reducing conditions at 800ºC, assuming a full (6-δ)-oxygen stoichiometry (δ = 0) for SMMO in air conditions. The TGA measurements were accomplished by rising temperature from RT to 800ºC under oxidizing condition (air), and then the atmosphere was switched to 10%H_2-Ar. TGA were performed by using a highly sensitive thermogravimetric equipment consisting of a symmetrical Cahn 1000 electrobalance and a symmetrical furnace (17). The thermobalance allows the determination of sample mass changes within ±10 μg at high temperatures for about 0.25 g powder samples of SMMA.

The oxidation state of Mo in doped (SMMNi) and non-doped (SMMO)-samples was evaluated by X-Ray photoelectron spectroscopy (XPS). The XPS were performed in a VG spectrometer equipped with Al-Kα radiation (hν =1486.6 eV) and a hemispherical electrostatic energy analyzer. XPS measurements were completed on SMMO and SMMNi samples before and after a thermal treatment under 10%H_2-Ar during 12 h.

Dense $Ce_{0.9}Gd_{0.1}O_{1.95}$ (GDC) pellets with thickness ~ 600 μm were used as electrolyte on symmetrical SMMO/GDC/SMMO and SMMNi/GDC/SMMNi cells. The

pellets were prepared by uniaxial pressing of commercial GDC powders and annealing in air at 1350ºC during 4 h. SMMO and SMMNi porous electrodes were deposited on both sides of the electrolyte by spin coating and calcination in air at 1000ºC for 3 h. EIS spectra were collected, using Pt-grids as current collectors, at 700ºC. EIS measurements were accomplished in a mix of dry H_2-Ar by increasing and subsequent decreasing the H_2 partial pressure (pH_2) from 0.05 to 1 atm. EIS spectra were collected by using an AUTOLAB PGSTAT30 potentiostat equipped with a frequency response analyzer (FRA) in a frequency range 10^6 to 10^{-3} Hz under a 50 mV amplitude signal and 0V bias voltage. Additionally, impedance measurements under humidified-H_2 (3% H_2O vapor) atmosphere were performed under the same experimental configuration.

Results and Discussion

Figure 1 shows XRD patterns for SMMO and SMMNi powders and their Rietveld refinements. The double perovskite phase was achieved for both compounds. XRD patterns were adjusted with triclinic *I-1* space group (18); the lattice parameters values are listed in Table I. These results indicate an expansion in the *a-b* plane due to the Mo-substitution by Ni. This effect could be associated to the Ni incorporation into the SMMO-structure, since the ionic radii of Ni^{+2}/Ni^{+3}(0.69/0.6 Å) is higher than that of Mo^{+6} (0.59 Å). Nevertheless, a net reduction in volume is caused by a contraction in the *c*-direction of the double perovskite structure. It may be due to an increase of the oxygen vacancies content.

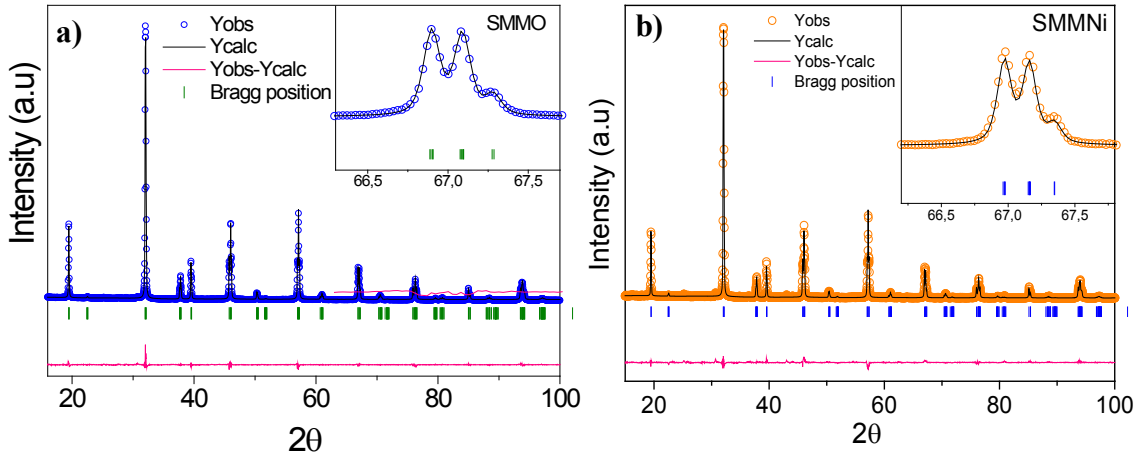

Figure 1. XRD patterns at room temperature and Rietveld refinements of **a)** SMMO and **b)** SMMNi.

TABLE I. Lattice parameters of SMMO and SMMNi compounds.

Parameters	SMMO	SMMNi
a(Å)	5.5762(4)	5.5846(7)
b (Å)	5.553(4)	5.5854(7)
c (Å)	7.9258(1)	7.8774(7)
Alpha	89.995(7)	89.997(11)
Beta	89.984(5)	90.000
Gamma	89.997(7)	89.726(5)
V (Å^3)	246.40(2)	245.71(5)

$R_p < 13$, $R_{wp} < 14$ and $\chi^2 < 3.4$

In Figure 2, the evolution of oxygen content (6-δ) with time for SMMO and SMMNi compounds at 800ºC under oxidizing (air) and reducing (10%H_2-Ar) conditions is shown. TGA results show that SMMO loses a small oxygen amount ($\Delta\delta \approx 0.06$) at 800ºC in reducing atmosphere. This result is in agreement with data reported by other authors (19-21). Meanwhile, the Mo-substitution by Ni in Sr_2MgMoO_6 compound creates oxygen vacancies in the structure under air environment. Similar to that observed for SMMO, the SMMNi compound under reducing atmosphere has an oxygen non-stoichiometry change of $\Delta\delta \approx 0.06$ which could be attributed to a change on the oxidation state of Mo and/or Ni.

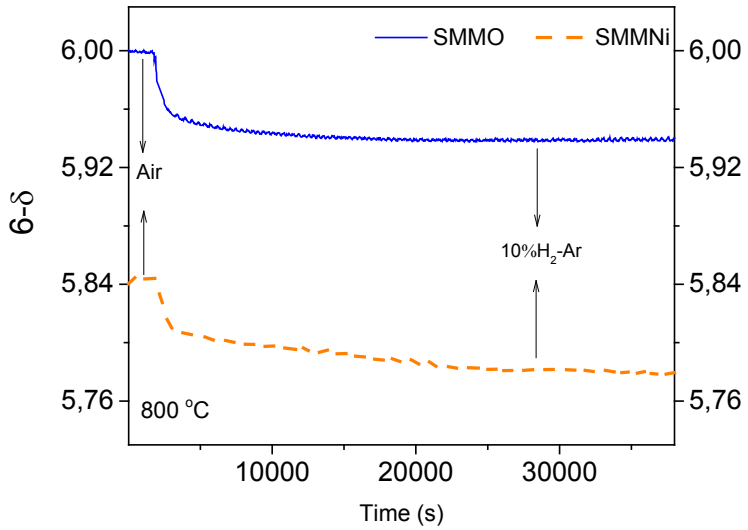

Figure 2. TG curves for SMMO and SMMNi compounds under oxidizing and reducing conditions at 800ºC.

XPS spectra of Mo for SMMO and SMMNi powders, before and after thermal treatment under 10%H_2-Ar at 800ºC, are depicted in Figure 3. The Mo-3d spectra display

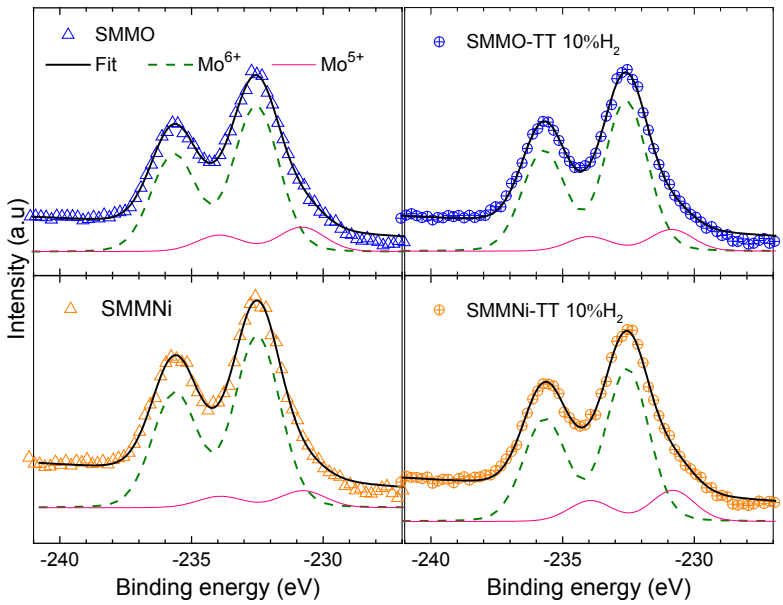

Figure 3. XPS spectra for the elements of **a)** Mo-3d before and after a thermal treatment under 10%H_2-Ar at 800ºC.

two peaks corresponding to spin-orbit split Mo-$3d_{5/2}$ and Mo-$3d_{3/2}$ sublevels. These peaks were fitted with a pair of doublets composed of Voight functions with fixed intensity ratio 3:2 separate by ~ 13 eV assigned to Mo^{6+} and Mo^{5+}. XPS spectra for Mo-3d of Sr_2MgMoO_6 powders are practically identical before and after the calcination in diluted-H_2 which would indicate that Mo does not change its oxidation state at the surface. The Mo^{6+} and Mo^{5+} coexistence could be surprising in the XPS spectrum for non-doped sample synthesized in air. This fact is in agreement with results reported by other authors for the SMMO compound (21-22). After the thermal treatment under 10% H_2-Ar, Mo^{5+} content in Ni-doped sample increases. It is noteworthy that the XPS analyses on Ni (not shown here) revealed that the oxidation state of Ni does not change after the annealing under reducing conditions.

Figure 4 shows the results of EIS spectra for SMMO and SMMNi at pH_2 of 0.05 atm before increasing pH_2.The anode polarization resistance (R_{pa}) for SMMNi is around 5 times higher than that determined for SMMO electrode. The abovementioned indicates that Ni-substitution by Mo in SMMO is detrimental for the R_{pa} values. The inset of Figure 4 displays the Bode diagrams for both compounds. It is important to note that R_{pa} for SMMO and SMMNi anodes decreases as the H_2-pressure increases from 0.05 to 1 atm. at 700ºC (not shown here). The samples were subjected to the maximum H_2-pressure (1 atm) condition at 700ºCduring ~2 h and then the H_2-pressure was decreased from 1 to 0.05 atm.

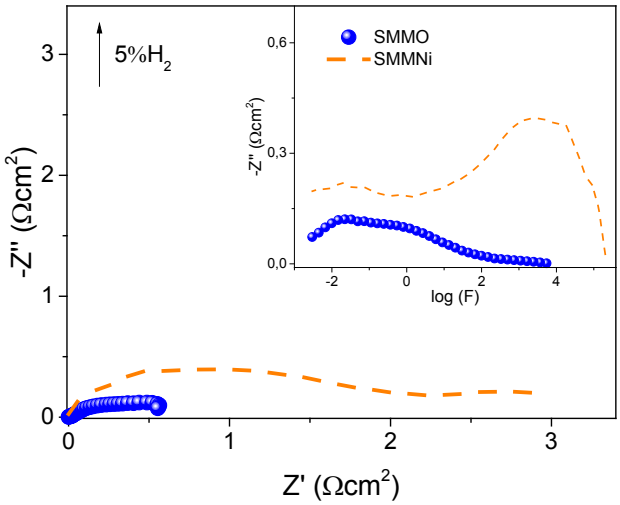

Figure 4. Impedance spectra of symmetrical SMMO/GDC/SMMO and SMMNi/GDC/SMMNi cells measured under 5%H_2-Ar at 700ºC, inset: Bode diagrams for symmetrical SMMO(SMMNi)/GDC/SMMO(SMMNi) cells.

As shown in Figure 5a, no significant difference was observed between the R_{pa} values measured under 100% and 5%H_2 for both compounds by decreasing pH_2. The Bode diagrams of EIS studies varying H_2-pressure are displayed in Figure 5b. This behavior of R_{pa} is completely different to those observed for other MIEC perovskite anodes such as $Sr(Ti_{0.3}Fe_{0.7})O_3$ and $(La,Sr)(Cr,Fe)O_3$ (23). For these perovskites, the authors proposed that, at high T and high pH_2, the anodic reaction is limited by a charge transfer process forming H_2O on the oxide surface with $R_{pa} = pH_2^{-1}$, whereas an activated dissociative hydrogen adsorption process ($R_{pa} = pH_2^{-0.5}$) becomes to be an important rate-limiting step, as temperature and pH_2 decreases. Impedance spectra of symmetrical

SMMO/GDC/SMMO and SMMNi/GDC/SMMNi cells under humidified-H_2 (3% H_2O vapor) are presented in Figure 6. The presence of H_2O vapor duplicates R_{pa} values of SMMO and SMMNi anodes. The R_{pa}values regardles pH_2, the increment of polarization resistance for Ni-doped sample (which displays a lower electrical conductivity in H_2 atmosphere than SMMO (24) and the fact that H_2O plays a limitating rol, are evidences of a complete different mechanim for H_2 oxidation in SMMO and SMMNi oxides, as compared with those of other perovskites anodes. More research is needed to clarify the origin of these differences.

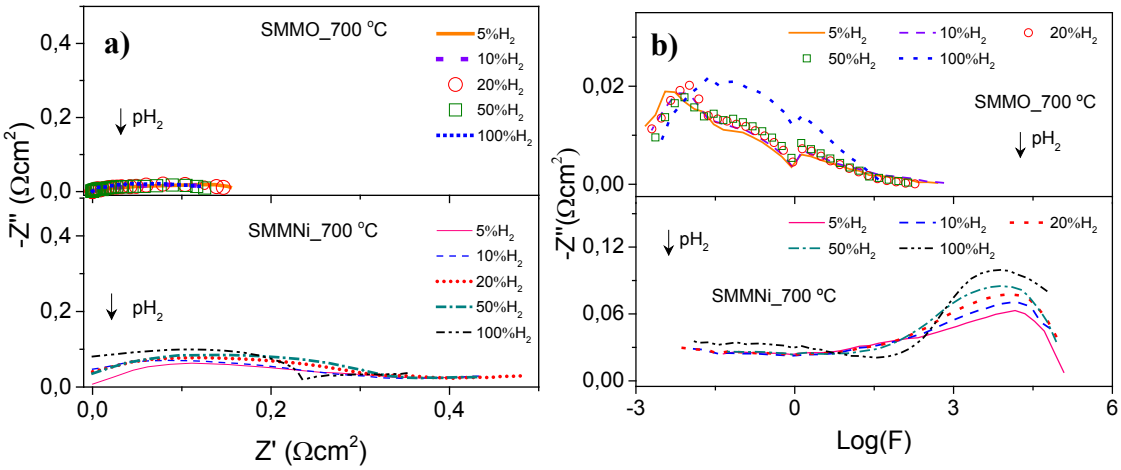

Figure 5. a) Impedance spectra of symmetrical SMMO/GDC/SMMO and SMMNi/GDC/SMMNi cells measured by decreasing the H_2-pressure at 700ºC; b) Bode diagrams for symmetrical cells decreasing H_2-pressure.

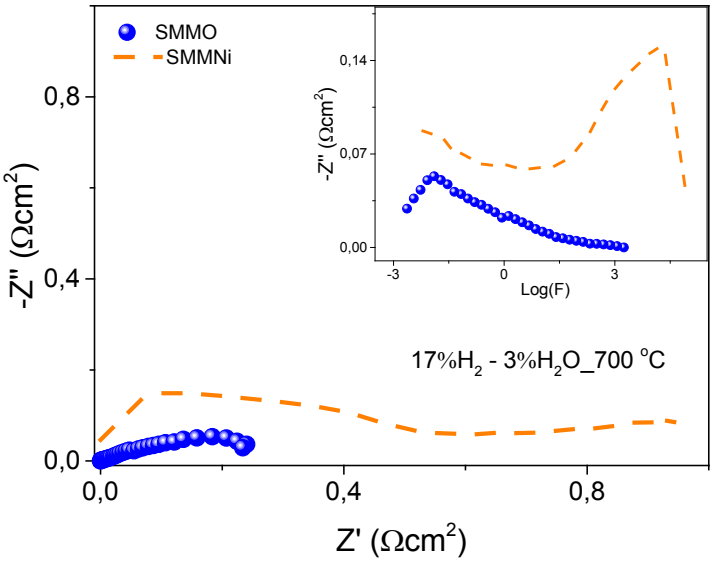

Figure 6. Impedance spectra of symmetrical SMMO/GDC/SMMO and SMMNi/GDC/SMMNi cells measured in 3% H_2O-vapor at 700ºC. Inset: corresponding Bode diagrams.

Conclusion

$Sr_2MgMo_{0.9}Ni_{0.1}O_{6-\delta}$ compound was synthesized by the combustion-solution method. SMMO and SMMNi powders display a triclinic structure. Ni-incorporation in

Sr_2MgMoO_6 compound creates oxygen vacancies under air condition. Mo^{6+}/Mo^{5+} are present in SMMO and SMMA powders before and after annealing in reducing environment. EIS experiments for varying the H_2-pressure at 700ºC indicate that, once the highest degree of reduction is reached for the SMMO(Ni) sample, the R_{pa} values does not change significantly decreasing pH_2.

Acknowledgments

The authors kindly acknowledge the support of CNEA, CONICET and Agencia Nacional de Promoción Científica y Tecnológica (ANPCyT) - PICT 2013-01032.

References

1. A. J. Jacobson, *Chem. Mater.*, **22** (3), 660 (2010).
2. M. Irshad, K. Siraj, R. Raza, A. Ali, P. Tiwari, B. Zhu, A. Rafique, A. Ali, M. Kaleem Ullah and A. Usman, *Appl. Sci.*, **6** (3), 75 (2016).
3. R. M. Ormerod, *Chem. Soc. Rev.,* **32**, 17 (2003).
4. J. B. Goodenough and Y.-H. Huang, *J. Power Sources*, **173** (1), 1 (2007).
5. M. Van Den Bossche and S. McIntosh, *J. Mater. Chem.*, **21** (20), 7443 (2011).
6. Y.-H. Huang, R.I. Dass, Z.-L. Xing and J.B. Goodenough, *Science*, **312** (5771), 254 (2006).
7. Y. Ji, Y.-H. Huang, J.-R. Ying and J.B. Goodenough, *Electrochem. Commun*., **9** (8), 1881 (2007).
8. D. Marrero-López, J. Peña-Martínez, J.C. Ruiz-Morales, M. Gabás, P. Núñez, M.A.G. Aranda and J.R. Ramos-Barrado, *Solid State Ionics*, **180** (40), 1672 (2010).
9. S. Vasala, M. Lehtimäki, S.C. Haw, J.M. Chen, R.S. Liu, H. Yamauchi, M. Karppinen, *Solid State Ionics*, **181** (15–16), 754 (2010).
10. M. J. Escudero, I. Gómez de Parada, A. Fuerte, and L. Daza, *J. Power Sources*, **243**, 654 (2013).
11. F. Wang, G. Zhong, S. Luo, L. Xia, L. Fang, and X. Song, *Catal. Commun*., **67**, 108 (2015).
12. K. Singh, S. A. Acharya, and S. S. Bhoga, *Indian Journal of Engineering & Materials Sciences*, **13**, 525 (2006).
13. M. Epifani, E. Melissano, G. Pace, and M. Schioppa, *J. Eur. Ceram. Soc.*, **27** (1), 115 (2007).
14. C. M. Chanquía, J. E. Vega-Castillo, A. L. Soldati, H. Troiani, and A. Caneiro, *J. Nanoparticle Res.*, **14** (9), 1104 (2012).
15. P. K. Dager, C. M. Chanquía, L. Mogni, and A. Caneiro, *Mater. Lett.*, **141**, 248 (2015).
16. J. C. Rodríguez, *Phys. B*, **192**, 55 (1993).
17. A. Caneiro, P. Bavdaz, J. Fouletier, and J. P. Abriata, *Rev. Sci. Instrum.*, **53** (7), 1072 (1982).
18. C. Bernuy-Lopez, M. Allix, C. Bridges, J. B. Claridge, and M. J. Rosseinsky, *Chem. Mater.*, **19** (5), 1035 (2007).
19. Y. Matsuda, M. Karppinen, Y. Yamazaki, and H. Yamauchi, *J. Solid State Chem.*, **182** (7), 1713 (2009).

20. S. Vasala, M. Lehtimäki, Y. H. Huang, H. Yamauchi, J. B. Goodenough, and M. Karppinen, *J. Solid State Chem.*, **183** (5), 1007 (2010).
21. D. Marrero-López, J. Peña-Martínez, J. C. Ruiz-Morales, D. Pérez-Coll, M. G. Aranda, and P. Núñez, *Mater. Res. Bull.*, **43** (8–9), 2441. (2008).
22. Z. Xie, H. Zhao, Z. Du, T. Chen, and N. Chen, *J. Phys. Chem. C*, **118**, 18853 (2014).
23. T. Zhu, D. E. Fowler, K. R. Poeppelmeier, M. Han, and S. A. Barnett, *J. Electrochem. Soc.*, **163** (8), F952 (2016).
24. P. K. Dager, L. Mogni, S. Soria, A. Caneiro, Study of the high temperature properties of $Sr_2MgMo_{0.9}A_{0.1}O_{6-\delta}$ (A = Co, Mn, and Ni), *under revision*.